

# Laboratory Report 4

## BETA-RAY SPECTROMETER

Kirsten Howley  
May 13, 2003

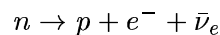
### ABSTRACT

In this experiment, the spectra of gamma rays resulting from nuclear transitions of  $\text{Na}^{22}$ ,  $\text{Cs}^{137}$ ,  $\text{Co}^{60}$ , and  $\text{Mn}^{54}$  are collected by means of their interaction with matter. By varying the source distance from the detector and the presence of various absorbers, different characteristics about the isotopes can be determined. These include the inverse square law, which was measured as  $d^{-1.7}$ , the absolute intensity of  $\text{Cs}^{137}$ , which was calculated to be  $305,000 \frac{\text{counts}}{\text{sec}}$ , and the mass attenuation coefficients of several materials.

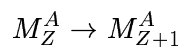
## 1. INTRODUCTION & THEORY

### 1.1. Beta Decay

Radioactive isotopes decay spontaneously as a result of an unstable nucleus. In this process, the nucleus transits from a less negative nuclear binding energy to a more negative nuclear binding energy. The difference in these two energies manifests itself in the release of electrons, positrons, neutrinos, and/or gamma rays. In  $\beta$  decay specifically, a neutron in the nucleus decays into a proton, electron, and an electron anti-neutrino:



The electrons emitted, with high kinetic energies, are referred to as beta rays. The resulting nucleus,  $M$ , is transformed:



where  $Z$  is the atomic number and  $A$  is the mass number. It was found experimentally that the electrons emitted in  $\beta$  decay were characterized by a range of kinetic energies up to that of the nuclear binding energy released. In order for that to be possible, it was theorized that another particle must exist to account for the missing energy. This new particle, the anti-neutrino,  $\bar{\nu}_e$ , satisfied the need for conservation of energy and momentum.

### 1.2. Beta Decay of Cesium 137

The excited state of Cesium decays to Barium with a half life of 30 years. For this reaction, two modes of decay exist: decay to the stable state of Barium (6.5% of occurrences) and decay to the excited state of Barium (93.5% of occurrences). The energy available to the created particles is 1,176 keV and 514 keV, respectively.

After Cesium has decayed to the excited state of Barium, the new nucleus undergoes further decay. This transition occurs by two different means. The most common decay, occurring 90% of the time, is to the stable state of Barium with the emission of a  $\gamma$ -ray<sup>1</sup> whose energy is equal to the difference between the excited and stable states of the Barium nucleus, a value of 662 keV. The less common decay, occurring only 10% of the time, is done by means of internal conversion. In this process, an electron is sucked into the excited nucleus and then kicked out with an energy equal to the difference between the excited and stable states of the Barium nucleus, minus the initial binding energy of the electron. These decay processes are summarized as follows:

- |   |  |         |
|---|--|---------|
| 1. ${}_{55}\text{Cs}^{137} \rightarrow {}_{56}\text{Ba}^{137} + \beta^- + \bar{\nu}_e$                      | $\Delta E = 1,176 \text{ keV}$                 | (6.5%)  |
| 2. ${}_{55}\text{Cs}^{137} \rightarrow {}_{56}\text{Ba}^{*137} + \beta^- + \bar{\nu}_e$                     | $\Delta E = 514 \text{ keV}$                   | (93.5%) |
| a. ${}_{56}\text{Ba}^{*137} \rightarrow {}_{56}\text{Ba}^{137} + \gamma$                                    | $\Delta E = 662 \text{ keV}$                   | (90%)   |
| b. ${}_{56}\text{Ba}^{*137} + e^-_{\text{bound}} \rightarrow {}_{56}\text{Ba}^{137} + e^-_{\text{unbound}}$ | $\Delta E = 662 \text{ keV} - E_{\text{bind}}$ | (10%)   |

The binding energy of the electron in the latter process is dependent on its initial orbital position in the atom. Thus, electrons absorbed from different orbital shells (i.e. k, l, & m) are emitted with differing energies. However, unlike the primary decays (1 & 2), these electron energies do not form a continuum, since in the latter transition (b) no particle accompanies the ejected electron and therefore the electron is forced to carry away any excess energy.

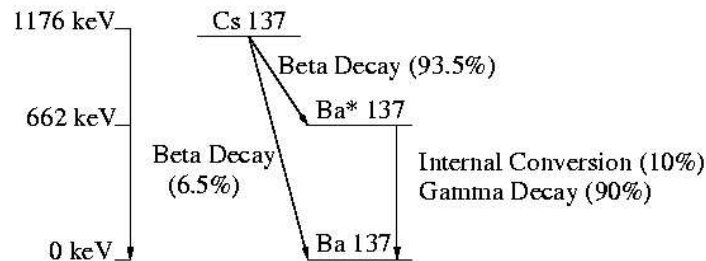


Fig. 1.—

### 1.3. The Decay Process

Gamma ray Spectroscopy focuses to measure the the energies of the high energy photons produced in nuclear transitions. Nuclei in excited states can move to lower energy states by means of beta decay, inverse beta decay or electron capture. A resulting by-product of these decay mechanisms is a gamma ray photon. Nuclei which make transitions via inverse beta decay also produce a positron, which then quickly annihilates with a local electron producing a characteristic energy equal to the rest mass of the two particles.

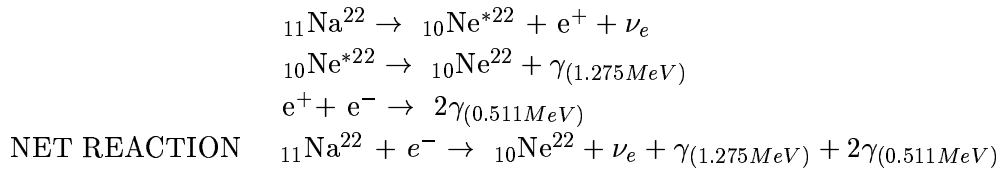
---

<sup>1</sup>A high energy photon.

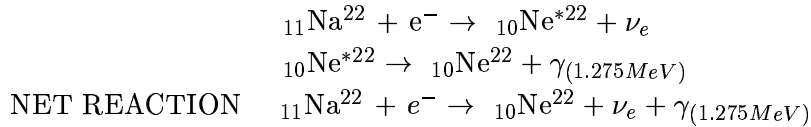
The radioactive species used in this experiment are Sodium 22, Cesium 137, Cobalt 60 and Manganese 54. The processes by which they decay and the resulting products are discussed in detail in the following sections.

### 1.3.1. Sodium 22 - ${}_{11}\text{Na}^{22}$

The excited state of Sodium decays to a stable form of Neon with a half life of 2.6 years. This end result is achieved predominantly by inverse beta decay (90% of incidences), but also by electron capture (10% of incidences). When the nuclei decays via inverse beta decay, a positron is produced. As a result, decay by this process results in two additional gamma rays of energy 511 MeV. The reaction for inverse beta decay is as follows:



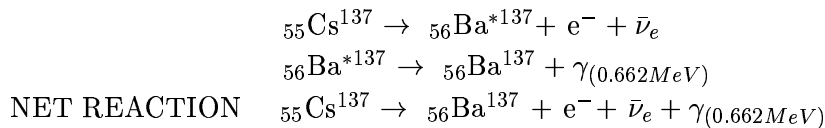
A small fraction of Sodium 22 decays through electron capture. In this process, the nucleus captures a nearby electron and decays. Since a positron is not produced, the 511 MeV gamma ray seen in the dominant reaction is not created. The process for electron capture in Sodium 22 is as follows:



As can be seen, both reactions produce a 1.275 MeV gamma ray, with two accompanying 511 MeV gamma rays, 90% of the time.

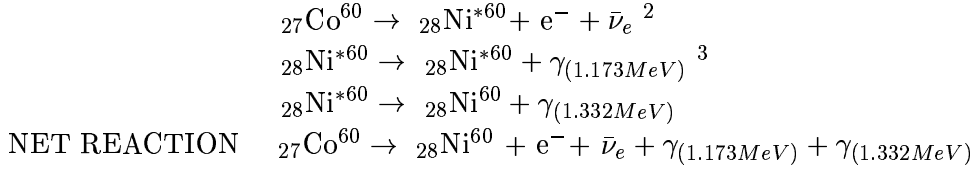
### 1.3.2. Cesium 137 - ${}_{55}\text{Cs}^{137}$

The excited state of Cesium decays to Barium with a half life of 30 years. This reaction occurs via beta decay. The process for this reaction is as follows:



### 1.3.3. Cobalt 60 - ${}_{27}\text{Co}^{60}$

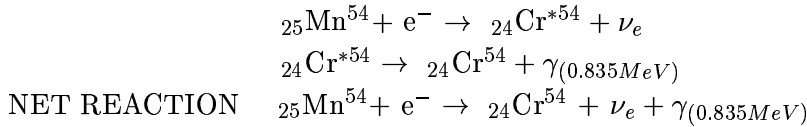
The excited state of Cobalt decays to a stable state of Nickel with a half life of 5.2 years. This end result is achieved when the nucleus beta decays to various forms of excited Nickel. The reaction that occurs over 99% of the time is as follows:



The other decay reactions, which occur less than 1% of the time, produce gamma rays with energies 0.83 MeV and 2.158 MeV.

### 1.3.4. Manganese 54 - ${}_{25}\text{Mn}^{54}$

The excited state of Manganese decays to a stable form of Chromium with a half life of 312 days. This is achieved solely by electron capture. The reaction is as follows:



## 2. EQUIPMENT & METHOD

The presence of gamma rays in this experiment is determined using the photoelectric effect, although Compton Scattering also occurs. Ideally, a gamma ray enters a thallium-doped sodium iodide [NaI(Tl)] crystal and is absorbed, thereby exciting and liberating an electron. This electron, with a high kinetic energy given by Equation 1, transfers its kinetic energy to neighboring electrons, thus exciting them as well. As the electrons fall back to their ground state, they emit visible photons. These photons are then received by a photomultiplier tube (PMT). As the photon enters the PMT it strikes a photo cathode thereby releasing an electron which is attracted to a local dynode with a high potential difference. The electron strikes the dynode and liberates more electrons, which are drawn to another dynode with a higher potential difference. This process repeats until the electrons reach the collector, at which point the current is converted into a voltage. Figure 2 demonstrates this process:

The number of electrons liberated in this process is a function of the voltage placed across the PMT tube. The voltage output of the PMT is proportional to the energy of the incident visible photons, and thus is proportional to the energy of the initial gamma ray. However, in order to determine the gain of the photomultiplier tube, the output PMT voltage had to be measured as a function of the voltage placed across the tube. To measure this, the output voltage of the PMT was fed into an external amplifier whose output was fed into a Pulse Height Analyzer (PHA). The external amplifier was necessary since the PHA is only capable of reading a signal up to 8 volts, with bin sizes corresponding to 1/256th of a volt.

Using the Cesium 137 isotope as a marker, the high voltage was varied across the PMT and the

---

<sup>2</sup>Where Ni\* produced has an ionization potential of 2.506 MeV

<sup>3</sup>Where Ni\* produced has an ionization potential of 1.332 MeV

Fig. 2.— Example of a visible photon leaving the NaI Scintillation Crystal and being converted into a voltage by the Photomultiplier Tube.

corresponding bin number on the PHA was recorded. Using the value of the external amplification and the size of the PHA bins, the output voltage of the PMT could be determined by employing the following conversion:

$$V_{out} = \frac{BinNumber \times \frac{1}{256}V}{Amplification}$$

By plotting the points and performing a least squares fit on the logarithmic values (see Figure 3), the gain of the PMT was determined to have a power dependence:

$$V_{out}(mV) = 0.76 \times [V_{in}(kV)]^{10.64}$$

This power dependence can easily be understood by referring back to Figure 2. The kinetic energy of a liberated electron in the PMT is dependent on the voltages placed on the dynodes. The higher the kinetic energy of an electron striking a dynode, the more electrons that are released. This results in an exponential increase in the net number of electrons which finally reach the anode.

In addition to the gain of the PMT, the linearity of the external amplifier needed to be determined. First, the saturation of the amplifier was measured. Using an input voltage of -1500V across the PMT and the Cesium 137 isotope as a marker, the external amplification was varied, and

Fig. 3.— Determining the relative gain of the PMT.

the corresponding bin number recorded. It was found that at approximately 100x amplification, the amplifier clipped. The results are plotted in Figure 4.

Next, the linearity of the amplifier was measured. This was done using a Pulse Generator and a *Kay Electric Co* attenuator. A 22 millisecond pulse was fed into the attenuator, whose output was fed into both an oscilloscope and an amplifier. The signal from the amplifier was then transmitted both to the oscilloscope and the PHA. This setup is shown in Figure 5.

The fine knob on the amplifier was set to 3, and the coarse adjustment was set to 4, 8, and 16; this corresponded to amplifications of 12, 24, and 48. The input pulse was varied using the attenuator, and the corresponding output voltages and bin numbers were recorded. Figure 6 demonstrates the non-linearity of the amplifier.

Since the values of the output pulses for identical input pulses did not double for doubled amplifications, it was determined that the amplifier was not functioning linearly. For this reason, the photopeaks in this lab were calibrated using the known energy values instead of gain and amplification conversions.

In addition to the capabilities of the amplifier, the abilities of the PHA was also investigated by determining the relationship between the rate of the pulse generator and the counts recorded by the PHA. The pulse rate was varied between 24  $\mu$ s and 6.4 ms. Rates below 24  $\mu$ s could not

Fig. 4.— Determining the saturation of the external amplifier.

be examined because PHA was unable to handle such high frequency signals; the PHA requires a finite time between signal processing. It was found that the counts under the peak on the PHA essentially increased as expected. Figure 7 demonstrates.

Once the capabilities and limitations of the equipment were established, data on the isotopes could be collected. A complete block diagram of the setup used for data acquisition is shown in Figure 8. The high voltage placed across the PMT was held at -1500 V.

### **3. DATA COLLECTION & ANALYSIS**

#### **3.1. Photopeaks, Backscatter Peaks, Pair Production Peaks, Compton Edges & Resolution**

The individual spectrums were recorded for the four isotopes, placed at a distance of 15 cm from the detector. The energy spectrums were calibrated on the PHA using the known values of the photopeaks for each source. From this data, the photopeaks, backscatter peaks, pair production peaks and Compton edges could be determined. Backscatter peaks occur when gamma rays interact with other surrounding materials prior to entering the detector. The gamma rays, which have been scattered through an angle of  $\pi$ , have a new energy corresponding to that given in Equation 4. In addition to the backscatter peaks, the location of the Compton edges can also be predicted using Equation 3.

Fig. 5.— Block diagram of setup for amplifier linearity determination.

The resolution represents the amount of fluctuation recorded around an incoming pulse. The tighter the distribution around the average energy of the incoming gamma ray, the better the resolution. The resolution can be computed by:

$$R = \frac{FWHM}{\bar{x}}$$

where R is the resolution, FWHM is the full width, half max value, and  $\bar{x}$  represents the photopeak value. If the FWHM value cannot be determined, but a Gaussian can be fit to the distribution, it can be estimated by:

$$FWHM = 2.35\sigma_x \tag{1}$$

Scintillation detectors usually have an energy resolution of 5-10%.

In the following sections, the predicted and measured values for each isotope are discussed, in addition to the resolution of the distributions.

### **3.1.1. Sodium 22 - ${}_{11}\text{Na}^{22}$**

The spectrum for Sodium 22 was recorded for a duration of 600 seconds at an amplification of 5x16 (80x). The spectrum was then calibrated using the photopeak, with a known energy of

Fig. 6.— Determining the linearity of the external amplifier.

1275 keV, and the pair production peak, with a known energy of 511 keV. After calibrating these points and performing a Gaussian fit, the photopeak was found to have a value of 1266 keV, the backscatter peak was found to have an energy of 124 keV, the pair production peaks were located at 506 keV, and the Compton edge was located at 287 keV. These results and their corresponding uncertainties are listed in Table 1.

Table 1: Spectra details for Sodium 22

	Photopeak	Pair Production Peak	Backscatter Peaks	Compton Edges
Predicted Peak (keV)	1275	511	170 & 213	340 & 1062
Measured Peak (keV)	$1266 \pm \sigma_x$	$506 \pm \sigma_x$	$124 \pm \sigma_x$	287
$\sigma_x$ (keV)	38	45	76	
FWHM (keV)	71	86	129	
Counts	$43,000 \pm 207$	$289,000 \pm 538$	$179,000 \pm 423$	
Resolution %	6	17	104	

It was anticipated that the measured photopeak and the pair production peak would closely match their predicted values, since these points were used to calibrate the spectrum. Two backscat-

Fig. 7.— Rate of Pulse Generator versus counts underneath photopeak on Pulse Height Analyzer.

ter peaks were anticipated in the spectrum; one for the pair production gamma rays and one for the photopeak corresponding to the isotope's nuclear transition. It appears that the backscatter peak corresponding to the pair production gamma rays resides at approximately 124 keV, instead of the predicted 170 keV. The backscatter peak expected at 213 keV for the 1275 keV gamma ray does not appear to be present, although it is possible that it has been overrun by the Compton edge located nearby. However, since the error quoted for the measured backscatter peak was quite large,  $124 \pm 76$ , it is possible that this measured peak actually encompasses both the backscattered gamma rays from pair production (predicted at 170 keV) and nuclear transitions (predicted at 213 keV).

In addition to two backscatter peaks, two Compton edges were predicted. The Compton edge corresponding to the pair production gamma rays was found to reside at 287 keV, instead of the predicted 340 keV. The Compton edge corresponding to the photopeak was barely visible, but upon close inspection of the spectrum can be approximated to lie somewhere between 1050 to 1100 keV; this range is close to the predicted Compton edge value of 1062 keV. The full spectrum, as well as isolated spectrums of the discussed peaks, can be found in Appendix A. The relevant features have been noted on the full spectrum.

Fig. 8.— Block diagram of setup used for data acquisition.

### ***3.1.2. Cesium 137 - ${}_{55}\text{Cs}^{137}$***

The spectrum for Cesium 137 was recorded for a duration of 600 seconds at an amplification of 7x16 (112x). The spectrum was calibrated using the photopeak, with a known energy of 662 keV, and the zero point. After calibrating these points and performing a Gaussian fit, the photopeak was found to have a value of 658 keV, the backscatter peak was found to have an energy of 179 keV, and

the Compton edge was located at approximately 454 keV. These results and their corresponding uncertainties are listed in Table 2.

Table 2: Spectra details for Cesium 137

	Photopeak	Backscatter Peak	Compton Edge
Predicted Peak (keV)	662	184	478
Measured Peak (keV)	$658 \pm \sigma_x$	$179 \pm \sigma_x$	454
$\sigma_x$ (keV)	48	74	
FWHM (keV)	85	130	
Counts	$366,000 \pm 605$	$347,000 \pm 589$	
Resolution %	13	73	

The measured and predicted values were found to be closely correlated. Although it was anticipated that the measured photopeak would closely match the predicted value (since it was used to calibrate the spectrum), it was surprising to find how closely correlated the predicted and measured values for the backscatter peak and Compton edge were.

In addition, there appears to be an additional peak located at approximately 800 keV in the spectrum. The source of this peak is unknown, although it is possible that it is a result of both a backscattered photon and an incoming gamma ray entering the detector simultaneously. This hypothesis is merely speculative though, since subsequent spectrums of Cesium 137 do not reveal such a peak.

To demonstrate the strength of backscattering, another spectrum of Cesium 137 was taken with a large Aluminum block placed behind the source. The backscatter peak was found to be a third as intense as the spectrum without the Aluminum block. This shows that strong interaction of the gamma rays with surrounding matter.

The full spectrum, as well as isolated spectrums of the discussed peaks, can be found in Appendix B. The relevant features have been noted on the full spectrum.

### 3.1.3. Cobalt 60 - ${}_{27}\text{Co}^{60}$

The spectrum for Cobalt 60 was recorded for a duration of 600 seconds at an amplification of 3x16 (48x). The spectrum was calibrated using the two photopeaks corresponding to the known values of 1173 keV and 1332 keV. After calibrating these points and performing a Gaussian fit, the first photopeak was found to have a value of 1154 keV, the second photopeak had an energy of 1307 keV, the backscatter peak was found to have an energy of 240 keV, and the Compton edge was located at approximately 917 keV. The results and their corresponding uncertainties are listed in Table 3.

Although two different backscatter peaks exist in theory for the two gamma rays, they are so

Table 3: Spectra details for Cobalt 60

	1st Photopeak	2nd Photopeak	Backscatter Peaks	Compton Edges
Predicted Peak (keV)	1173	1332	210 & 214	963 & 1118
Measured Peak (keV)	$1154 \pm \sigma_x$	$1307 \pm \sigma_x$	$240 \pm \sigma_x$	917
$\sigma_x$ (keV)	119	91	28	
FWHM (keV)	n/a	n/a	28	
Counts	$86,000 \pm 293$	$51,000 \pm 226$	$19,000 \pm 138$	
Resolution %	24	16	12	

close in energy values (differing by only 4 keV) that it is impossible to resolve them in the spectrum. In contrast, the two Compton edges have a much larger energy difference. However, the Compton edge for the 1332 keV gamma ray corresponds to a value of 1118 keV, which lies in close proximity to the 1173 keV photopeak. It is likely that this second Compton edge is masked by this photopeak and therefore is not seen in the spectrum. The full spectrum, as well as isolated spectrums of the discussed peaks, can be found in Appendix C. The relevant features have been noted on the full spectrum.

Since the two photopeaks overlapped, *Analyze* was unable to determine the FWHM value. Therefore, in order to calculate the resolution, Equation 5 was employed to estimate the FWHM of each photopeak.

### 3.1.4. Manganese 54 - ${}_{25}\text{Mn}^{54}$

The spectrum for Manganese 54 was recorded for a duration of 6000 seconds at an amplification of 6x16 (96x). Data was acquired for a longer period of time because of the short half-life of Manganese. The spectrum was calibrated using the photopeak, with a known energy of 835 keV, and the zero point. After calibrating these points and performing a Gaussian fit, the photopeak was found to have a value of 834 keV, the backscatter peak was found to have an energy of 172 keV, and the Compton edge was located at approximately 772 keV. These results and their corresponding uncertainties are listed in Table 4.

The measured and predicted values were found to be closely correlated. Again, this was anticipated for the photopeak since it was used to calibrate the spectrum. The full spectrum, as well as isolated spectrums of the discussed peaks, can be found in Appendix D. The relevant features have been noted on the full spectrum.

### 3.2. Inverse Square Law

Unlike beta rays, gamma rays are characterized to have an intensity that is inversely proportional to the square of the distance from the source. To demonstrate this dependence, spectrums were collected for varying distances. The source was placed at 6, 9, and 12 inches from the detector, and data was acquired for 600 secs at an amplification of 7x16 (112x). For each spectrum, the number of counts under the photopeak distribution was collected and plotted against its distance

Table 4: Spectra details for Manganese 54

	Photopeak	Backscatter Peak	Compton Edge
Predicted Peak (keV)	835	196	639
Measured Peak (keV)	$834 \pm \sigma_x$	$172 \pm \sigma_x$	596
$\sigma_x$ (keV)	52	74	
FWHM (keV)	98	n/a	
Counts	$110,000 \pm 332$	$87,000 \pm 295$	
Resolution %	12	101	

from the detector. Figure 9 shows the dependence:

Fig. 9.— Demonstrating the Inverse Square Law.

Although the inverse square law did not have the exact  $d^{-2}$  dependence anticipated, the value of  $d^{-1.7}$  was quite close. Reasons for the deviation from the actual dependence can be attributed to limitations of the equipment in recording intensities and errors in measuring the distance from the detector. However, it is clear from Figure 9 that these errors must be systematic, since the measured points lie closely on the fitted line. The spectrums obtained in verifying this dependence can be found in Appendix E.

### 3.3. Absolute Intensity of Cesium 137

Since the intensity of the isotopes is measured at some distance, it is difficult to measure directly the absolute intensity of a source at  $d=0$ . In order to compute the absolute intensity of Cesium 137, measured intensities had to be converted. This was achieved by the following equation:

$$I_{measured} = I_{absolute} \left[ n(E) \frac{\Delta\Omega}{4\pi} \right]$$

where  $n(E)$  is the intrinsic efficiency and  $\Delta\Omega$  represents the solid angle. Using the NaI literature, the value of quantity given in brackets was determined to be 0.2%, given a NaI crystal thickness of  $1\frac{1}{4}$ " , an incoming gamma ray of 0.662 MeV, and a source distance of 15 cm from the detector.

A Cesium 137 spectrum was taken for 600 seconds at a distance of 15 cm from the detector at an amplification of 7x16 (122x), with great care to ensure that interaction with surrounding media was minimized. The dark current was also taken and subsequently subtracted off the acquired spectrum. Careful calibration of the spectrum yielded 366,000 net counts underneath the photopeak, corresponding to an  $I_{measured}$  of 610 counts/sec. This translates into an  $I_{absolute}$  of 305,000  $\pm$  12,000 counts/sec.

### 3.4. Mass Attenuation Coefficient

When gamma rays are funneled through a narrow beam and pass through an absorber of variable thickness, an attenuation of the gamma ray intensity results. The gamma rays are either absorbed, scattering or transmitted through the medium. The intensity of the transmitted rays,  $I$ , is given by:

$$\frac{I}{I_0} = e^{-\mu t}$$

where  $\mu$  is the linear attenuation coefficient defined by probabilities of transmission, and  $t$  is the thickness of the medium. However, a much more commonly used coefficient is the mass attenuation coefficient given by:

$$\text{Mass Attenuation Coefficient (MAC)} = \frac{\mu}{\rho}$$

where  $\rho$  is the density of the material. This coefficient is not a function of the thickness of the material, and therefore can be determined by measuring the intensity of gamma rays penetrating materials of varying thickness.

The mass attenuation coefficient was measured for Sodium 22 and Cesium 137. Aluminum, Copper and Lead of variable thicknesses were used as absorbers. The source was placed 32 cm away from the detector with thick lead bricks located at 8 and 24 cm from the source. An absorber was then placed between the two lead bricks, and the spectrums were collected. In addition, a spectrum without an absorber was acquired in order to obtain the value of  $I_0$ . Figure 10 plots the results for Sodium 22 and Figure 11 for Cesium 137.

Fig. 10.— Determining the linear attenuation coefficients for Sodium 22 using Al, Cu and Pb.

The linear attenuation coefficient was computed by fitting a straight line to the equation:

$$\ln\left(\frac{I}{I_0}\right) = -\mu t$$

Once this value was obtained, dividing by the density of the medium used yielded the desired mass attenuation coefficient for each isotope. Table 5 lists the results:

Table 5: Mass Attenuation Coefficients

Isotope	Absorber	Density $\frac{g}{cm^3}$	$\mu\left(\frac{1}{mm}\right)$	MAC $\left(\frac{cm^2}{g}\right)$	MAC $\left(\frac{cm^2}{mg}\right)$
Na <sup>22</sup>	Al	2.7	0.014	0.005	0.00005
Na <sup>22</sup>	Cu	9.0	0.039	0.043	0.000043
Na <sup>22</sup>	Pb	11.3	0.093	0.082	0.000082
Cs <sup>137</sup>	Al	2.7	0.022	0.081	0.000081
Cs <sup>137</sup>	Cu	9.0	0.065	0.072	0.000072
Cs <sup>137</sup>	Pb	11.3	0.510	0.451	0.000451

Fig. 11.— Determining the linear attenuation coefficients for Cesium 137 using Al, Cu and Pb.

#### 4. CONCLUSIONS

General conclusions can be drawn about the nature of the spectra resulting from nuclear transitions. First, certain features are characteristic in each of the spectra obtained for  $\text{Na}^{22}$ ,  $\text{Cs}^{137}$ ,  $\text{Co}^{60}$ , and  $\text{Mn}^{54}$ ; these features include photopeaks corresponding to the gamma rays emitted by the nuclear transitions, strong Compton scattering of the gamma rays, and backscatter peaks formed by interactions with surrounding media. Unfortunately, the resolution of the peaks was poor, although calibration of the features still reasonable mimicked predicted values.

The inverse square law anticipated for gamma ray intensity was found to be  $d^{-1.7}$ . Although this number deviates from the true value of  $d^{-2}$ , it is reasonably close to this power law. Many sources of possible errors exist, including distance calibration errors, instrumentation limitations in collecting counts, gamma ray interaction with surrounding media, etc. Given these interferences, the obtained relation was quite satisfactory.

The determination of the absolute intensity of Cesium 137 yielded a value of  $I_{absolute} = 305,000 \pm 12,000$  counts/sec. The error quote on this value reflects the error of  $I_{measured}$ , or by Poisson statistics an error value of  $\sqrt{(I_{measured})}$ . This value was used because we are interested in the accuracy of the mean number of absolute counts, not its distribution about the mean value.

The mass attenuation coefficients for Aluminum, Copper and Lead were also acquired for

incident radiation of 662 keV ( $\text{Cs}^{137}$ ) and 1275 keV ( $\text{Na}^{22}$ ). Aluminum was found to have mass attenuation coefficients ( $\frac{\text{cm}^2}{\text{g}}$ ) of 0.081 & 0.005, Copper had 0.072 & 0.043, and Lead had 0.451 & 0.082, for  $\text{Cs}^{137}$  and  $\text{Na}^{22}$  gamma rays, respectively.

Although quite a large sum of data was collected for this lab, the intent of the experiment was to become familiar with the equipment. It was found that the amplifier used in this experiment was quite poor, and possibly needs to be replaced. An understanding of the various methods in which gamma rays interact with matter was also key in decomposing the resulting spectra. Overall, this experiment greatly and equally incorporated theory, equipment and data analysis abilities for its performance.

## 5. APPENDIX A

## 6. APPENDIX B

## 7. APPENDIX C

## 8. APPENDIX D

## 9. APPENDIX E

## 10. REFERENCES

Knoll, *Radiation Detection and Measurement*, John Wiley and Sons, New York, 1979. #QC787.C6.K56, 16-25, 62-71, 78-95, 272-284, 306-338.